

Tunable magnetism in bilayer transition metal dichalcogenides

Li-Ya Qiao,^{1,*} Xiu-Cai Jiang,^{1,*} Ze Ruan,¹ and Yu-Zhong Zhang^{1,†}

¹*Shanghai Key Laboratory of Special Artificial Microstructure Materials and Technology,
School of Physics Science and Engineering, Tongji University, Shanghai 200092, P.R. China*

(Dated: April 19, 2024)

Twist between neighboring layers and variation of interlayer distance are two extra ways to control the physical properties of stacked two-dimensional van der Waals materials without alteration of chemical compositions or application of external fields, compared to their monolayer counterparts. In this work, we explored the dependence of the magnetic states of the untwisted and twisted bilayer 1T-VX₂ (X = S, Se) on the interlayer distance by density functional theory calculations. We find that, while a magnetic phase transition occurs from interlayer ferromagnetism to interlayer antiferromagnetism either as a function of decreasing interlayer distance for the untwisted bilayer 1T-VX₂ or after twist, richer magnetic phase transitions consecutively take place for the twisted bilayer 1T-VX₂ as interlayer distance is gradually reduced. Besides, the critical pressures for the phase transition are greatly reduced in twisted bilayer 1T-VX₂ compared with the untwisted case. We derived the Heisenberg model with intralayer and interlayer exchange couplings to comprehend the emergence of various magnetic states. Our results point out an easy access towards tunable two-dimensional magnets.

I. INTRODUCTION

The breakthroughs in discovering several layered two-dimensional van der Waals magnets, for example, Cr₂Ge₂Te₆¹, CrI₃², Fe₃GeTe₂³, FePS₃⁴, VX₂ (X=Se, S)^{5,6}, etc., have stimulated tremendous research interest, due to their potential applications as high-performance functional nanomaterials^{7,8} and the flexible tunability via changing external controlling parameters, such as twist⁹, pressure¹⁰, strain^{11,12}, magnetic field^{13,14}, electric field¹⁵, doping¹⁶, stacking order¹⁷, and introducing defects^{18,19}, etc.

Recently, great efforts have been devoted to tuning the magnetism of VX₂ using various approaches. It has been theoretically pointed out that strain can induce tunable magnetism in VX₂^{11,12}. Using first-principles calculations, it was shown that the magnetism will increase sharply when monolayer VS₂ is exfoliated from the bulk at room temperature²⁰. Additionally, there has been a proposal for tunable magnetic phase transitions from interlayer ferromagnetic to antiferromagnetic states in bilayer VX₂ under pressure²¹. Moreover, stacking order has been recognized as an effective way to tune interlayer magnetic orders in bilayer VSe₂²². Finally, it was discovered that ferroelectricity and antiferromagnetism can be coupled through a ferrovalley in bilayer VS₂, enabling electrically controlled magnetism²³. Apart from these theoretical calculations, experiments have demonstrated that Se vacancies^{19,24} can enhance the magnetism, and the deposition of Co²⁵ or Fe²⁶ can induce the magnetism in VSe₂.

Despite extensive investigations, the magnetism of twisted bilayer VX₂ under pressure remains unexplored. It is known that twist and pressure both can tailor the properties of layered materials due to the corresponding variation of interlayer couplings^{27,28}. As a result, many fascinating phenomena arise, such as pressure-dependent flat bands^{29,30} and band gap^{31,32}, angle-dependent renor-

malized Fermi velocity^{33,34}, twist-induced site-selective phases³⁵, etc. In addition to these phenomena, the magnetism of materials is greatly influenced by interlayer couplings as well. For instance, interlayer ferromagnetic and antiferromagnetic states coexist in twisted bilayer CrI₃, which results from a competition between the interlayer coupling and the energy cost for forming ferromagnetic-antiferromagnetic domain walls³⁶. Therefore, it is foreseeable that magnetic phase transitions may also emerge in bilayer VX₂ when taking both twist and pressure into consideration.

In this paper, we investigate the tunability of magnetism with decreasing interlayer distances, which can be effectively viewed as increasing pressure, in both untwisted and twisted bilayer 1T-VX₂, whose monolayer counterpart has been experimentally synthesized^{5,37}. We find that a phase transition from ferromagnetic state (FM) to layered antiferromagnetic state (LAFM) occurs in untwisted bilayer 1T-VX₂ as interlayer distance decreases, where intralayer magnetic order remains ferromagnetic while interlayer becomes antiferromagnetic. The estimated critical pressures for the phase transition of bilayer 1T-VSe₂ and bilayer 1T-VS₂ are 36.21 GPa and 42.65 GPa, respectively. Using a simple Heisenberg model, we ascribe this phase transition to the competition between the nearest- and next-nearest-neighbor interlayer couplings, where the former, supporting FM, plays a leading role at large interlayer distances while the latter, favoring LAFM, plays a dominant role at small interlayer distances. To investigate the tunability of magnetism in bilayer 1T-VX₂ under both twist and pressure, we then take the case with a twisted angle of $\theta = 21.79^\circ$ as an example since it corresponds to the smallest commensurate supercell. Although we have only investigated the smallest commensurate supercell here, it is worthwhile to mention that there exist many other twisted angles with commensurate supercells that can be accessed with DFT as shown in the TABLE 1 of the Supplemental

Material³⁸. It is found that a phase transition from FM to LAFM occurs in bilayer 1T-VX₂ under twist solely. Remarkably, richer magnetic phase transitions are found under pressure and the critical pressures for the phase transition are greatly reduced in twisted bilayer 1T-VX₂ compared with the untwisted case, where twisted bilayer 1T-VSe₂ undergoes phase transitions of LAFM-AFM1-AFM2 while twisted bilayer 1T-VS₂ experiences phase transitions of LAFM-FM-AFM2 as interlayer distance is reduced. The critical pressures for the first and second phase transitions in twisted bilayer 1T-VSe₂ are 7.055 GPa and 20.73 GPa, respectively, while those in twisted bilayer 1T-VS₂ are 13.91 GPa and 32.21 GPa, respectively. Here, AFM1 and AFM2 are two novel magnetic states characterized by both intralayer antiferromagnetic and interlayer ferromagnetic orders. For AFM1, the spins of overlapping V atoms (from the top view) are antiparallel to the rests of the same layer, while for AFM2, spins of some non-overlapping V atoms (from the top view) are parallel to that of overlapping V atoms as shown in Fig. 3(b). By treating the non-overlapping V atoms with C_3 rotational symmetry in the supercell at each layer as a pseudo-atom with a large effective magnetic moment, an effective Heisenberg model is derived to understand these magnetic phase transitions. Please note, our aim is to extract a minimal model to comprehend tunable magnetism we discovered by DFT calculations in the twisted bilayer 1T-VX₂ of 21.79°, rather than to create a unified model for all twisted angles which is out of the scope of our study. Using this model, we find that the competition and cooperation between intralayer and interlayer couplings are responsible for the rich magnetic phase transitions in twisted bilayer 1T-VX₂.

The structure of our paper is organized as follows. Section II describes the details of the structure and the method we used. Section III presents our main results, including the magnetic phase transitions and the superexchange couplings as functions of interlayer distances for both untwisted and twisted bilayer 1T-VX₂, the schematic diagram of magnetic phase transitions in the twisted bilayer 1T-VX₂ as interlayer distance decreases, the structure of the twisted bilayer 1T-VX₂ and its modelling. Section IV presents a detailed discussion about our results, and Section V concludes with a summary.

II. COMPUTATIONAL METHOD

Our density functional theory calculations are based on the projector-augmented-wave method³⁹, as implemented in the Vienna *ab initio* simulation package^{40,41}. We choose the generalized gradient approximation of Perdew-Burke-Ernzerhof⁴² as the exchange-correlation functional with the van der Waals correction of DFT-D2 developed by Grimme⁴³. A plane-wave energy cutoff of 450 eV is employed. A sufficiently large vacuum distance of 20 Å is used to eliminate the interactions between peri-

odic images of the layers in the direction perpendicular to the plane. The Brillouin-zone integration is carried out with Γ -centered K-point grids of $9 \times 9 \times 1$ and $25 \times 25 \times 1$ for twisted bilayer 1T-VX₂ and untwisted bilayer 1T-VX₂, respectively. The convergence criteria for the energy and atomic forces are 1×10^{-6} eV and 0.01 eV/Å, respectively. We adopt the GGA+ U approach of Dudarev⁴⁴ to include the effective on-site Coulomb interactions U_{eff} between electrons of d orbitals in V atoms, where $U_{eff} = 1$ eV is adopted since the fully optimized in-plane lattice constants are comparable with the experiment^{45,46} with $a = b = 3.317 \text{ Å}$ ($a = b = 3.189 \text{ Å}$) for 1T-VSe₂ (1T-VS₂).

III. RESULTS

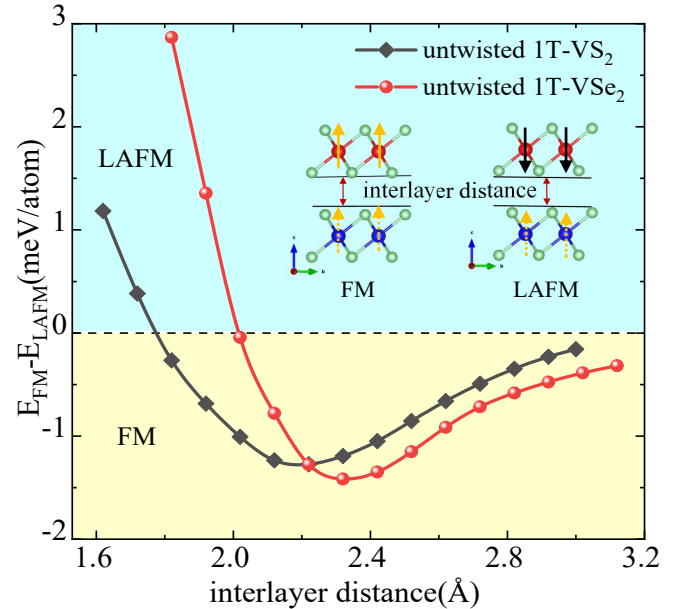


FIG. 1. The energy difference between FM and LAFM $E_{FM} - E_{LAFM}$ as a function of the interlayer distance for untwisted 1T-VX₂. The inset demonstrates the specific configurations of FM and LAFM, where orange dot arrow and orange (black) line arrow denote the spin up in the bottom layer and the spin up (down) in the top layer, respectively.

As pressure can tune the magnetism, we will now explore the tunability of magnetism in untwisted bilayer 1T-VX₂ with decreasing interlayer distances corresponding to increasing pressure. In Fig. 1, we present the evolution of energy difference between FM and LAFM as a function of the interlayer distance for untwisted 1T-VX₂. As can be seen, a magnetic phase transition from interlayer FM to LAFM occurs in both bilayer 1T-VSe₂ and bilayer 1T-VS₂ with the decrease of interlayer distance, which is consistent with previous study²¹. Part of our results, such as the stability of the magnetic ground states, is double-checked by DS-PAW which is also based on the projector-augmented-wave method³⁹.

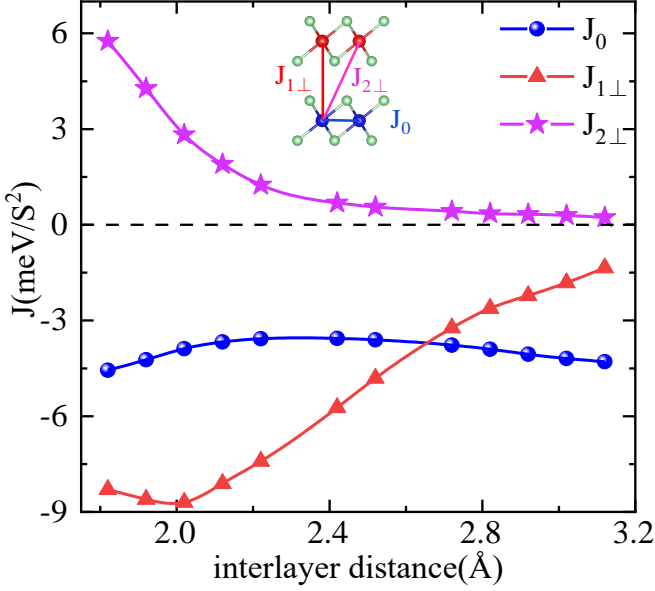


FIG. 2. The superexchange couplings in untwisted 1T-VSe₂ as functions of the interlayer distance. The nearest-neighbor intralayer coupling J_0 , nearest-neighbor interlayer coupling $J_{1\perp}$, and next-nearest-neighbor interlayer coupling $J_{2\perp}$ are illustrated in the inset.

To gain a deeper insight into the underlying physics of this magnetic phase transition, a simple Heisenberg model $H = E_0 + \sum_{ij} J_{ij} \mathbf{S}_i \cdot \mathbf{S}_j$ is employed to describe the magnetic properties of bilayer 1T-VSe₂, where E_0 is the ground state energy independent of the spin configuration and J_{ij} is the superexchange coupling between local V moments of \mathbf{S}_i and \mathbf{S}_j . Based on the energy differences among four magnetic states provided in the Supplemental Material (see Fig.S3)³⁸, the nearest-neighbor intralayer coupling J_0 , nearest-neighbor interlayer coupling $J_{1\perp}$, and next-nearest-neighbor interlayer coupling $J_{2\perp}$ are derived and are summarized in Fig.2. Obviously, J_0 remains ferromagnetic, leading to the intralayer ferromagnetism at all interlayer distances. In contrast, the interlayer magnetic order changes from ferromagnetic to antiferromagnetic with the decrease of interlayer distance due to the competition between $J_{1\perp}$ and $J_{2\perp}$. At small interlayer distances where $J_{1\perp} > -3J_{2\perp}$, LAFM appears. Otherwise, FM remains. Thus, compressing interlayer distances, viewed as applying pressure, can tune interlayer couplings which may induce a magnetic phase transition in untwisted bilayer 1T-VX₂.

Since twist can tune the interlayer couplings as well, the twisted bilayer 1T-VX₂ may exhibit richer magnetic phase transitions than the untwisted one. We then explore the tunability of magnetism in twisted bilayer 1T-VX₂ (X= S, Se) with decreasing interlayer distances. The twisted angle is set to be $\theta = 21.79^\circ$ and the twisted center locates at two overlapping V atoms [see the structure in Fig.4(a)]. As the system exhibits C_3 rotational symmetry based on the following points: $(0,0)$, $(a/3, 2b/3)$,

and $(2a/3, b/3)$, we investigated 20 possible magnetic configurations consistent with the rotational symmetry of the system as shown in Fig.S4 of the Supplemental Material³⁸. Figure3(a) presents the schematic diagram of magnetic phase transitions in twisted bilayer 1T-VX₂ as a function of interlayer distance. First, it can be seen that a phase transition from FM to LAFM occurs in bilayer 1T-VX₂ under twist solely (the interlayer distances of bilayer 1T-VSe₂ and bilayer 1T-VS₂ without compression are of 3.12 Å and 3.0 Å, respectively). Remarkably, richer magnetic phase transitions appear in twisted bilayer 1T-VX₂ compared with the untwisted case as interlayer distances decrease, where twisted bilayer 1T-VSe₂ undergoes phase transitions of LAFM-AFM1-AFM2 while twisted bilayer 1T-VS₂ experiences phase transitions of LAFM-FM-AFM2. Here, AFM1 and AFM2 are characterized by both intralayer antiferromagnetic and interlayer ferromagnetic orders as shown in Fig.3(b). While, for AFM1, the spins of overlapping V atoms (from the top view) are antiparallel to the rests in the same layer, for AFM2, spins of some non-overlapping V atoms (from the top view) are parallel to that of overlapping V atoms.

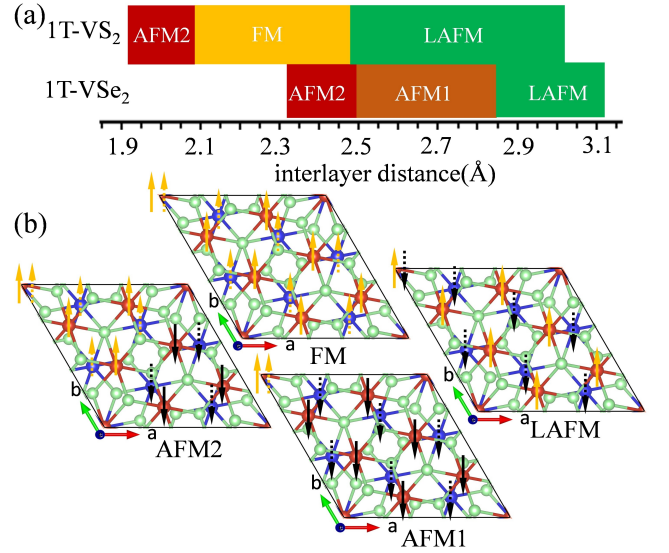


FIG. 3. (a) The schematic diagram of magnetic phase transitions in the twisted bilayer 1T-VS₂ and 1T-VSe₂ as functions of interlayer distance. (b) The specific configurations of LAFM, FM, AFM1, AFM2, where orange (black) dot arrow and orange (black) line arrow denote the spin up (down) in the bottom layer and the spin up (down) in the top layer, respectively.

To investigate the underlying physics of the magnetic phase transitions in twisted bilayer 1T-VX₂, we will now map twisted bilayer 1T-VX₂ onto an effective lattice and establish an effective Heisenberg model based on this lattice. According to the C_3 rotational symmetry of the system, we identify three distinct regions of V atoms within the supercell at each layer, namely regions A, O1, and O2, where both O1 and O2 include three equivalent V

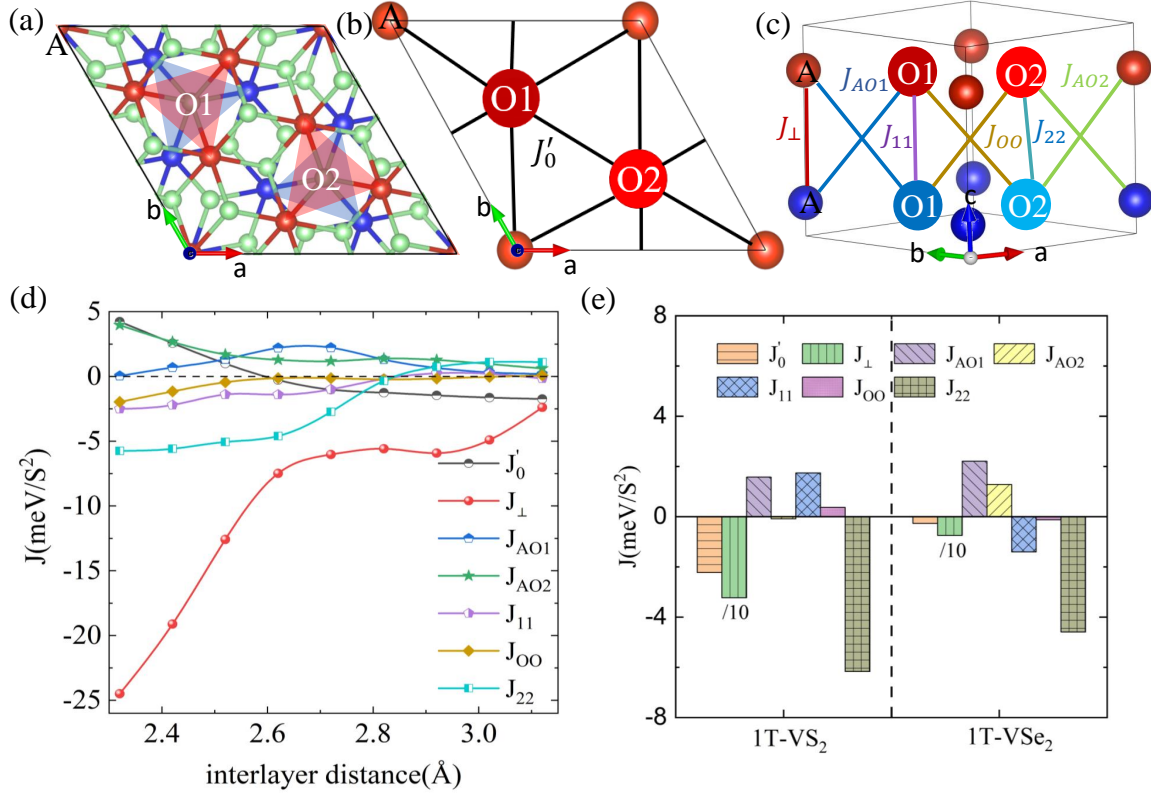


FIG. 4. (a) The top view of twisted bilayer 1T-VX₂ with twisted angle of $\theta = 21.79^\circ$, where the red, blue, and green balls denote V atoms in the top layer, V atoms in the bottom layer, and X atoms, respectively. By treating the total magnetic moment of three non-overlap V atoms with C_3 rotational symmetry [locate at the vertexes of each triangle in (a)] in the supercell at each layer as an effective magnetic moment, twisted bilayer 1T-VX₂ can be mapped onto an effective AA stacking bilayer triangular lattice. The top view (b) and side view (c) of the effective AA stacking bilayer triangular lattice, where the intralayer nearest-neighbor coupling J'_0 is shown in (b) and interlayer couplings J_\perp , J_{AO1} , J_{AO2} , J_{11} , J_{OO} , and J_{22} are presented in (c). (d) The superexchange couplings J'_0 , J_\perp , J_{AO1} , J_{AO2} , J_{11} , J_{OO} , and J_{22} as functions of interlayer distance. (e) The superexchange couplings of twisted bilayer 1T-VS₂ and 1T-VSe₂ at interlayer distance of 2.32 Å and 2.62 Å, respectively

atoms located at the vertexes of each triangle as shown in Fig.4(a). Besides, the magnetic moment on each V atom remains approximately $1\mu_B$ irrespective of magnetic orders. Thus, we can treat the total magnetic moment of V atoms in region O1 (O2) within the supercell at each layer as an effective magnetic moment that is three times larger than the original moment of each V atom. Ultimately, the twisted bilayer 1T-VX₂ is mapped onto an effective AA stacking bilayer triangular lattice which includes three inequivalent sublattices at each layer, namely A, O1, and O2, as presented in Fig.4(b) and 4(c). By taking into account the nearest-neighbor intralayer coupling, nearest-neighbor interlayer couplings, and next-nearest-neighbor interlayer couplings, we obtain an effective Heisenberg model for this effective AA stacking bilayer triangular lattice that consists of J'_0 , J_\perp , J_{AO1} , J_{AO2} , J_{11} , J_{OO} , and J_{22} as shown in Fig.4(b) and 4(c). Please note that, by carefully examining the relationship between the Heisenberg model of the original lattice and the Heisenberg model of the effective bilayer triangular lattice, it can be found that, although the A, O1, and

O2 sites are inequivalent, the nearest-neighbor intralayer couplings between any two of them are equal. In addition, based on the fact that both the magnetic state of monolayer VX₂ and the magnetic phase transition of untwisted bilayer 1T-VX₂ can be well understood by merely involving the nearest-neighbor intralayer exchange coupling J_0 and twist between layers will not change the paths for spin exchanges between two intralayer vanadium atoms, it is reasonable to infer that inclusion of intralayer exchange coupling up to nearest neighbor is sufficient for modelling the twisted bilayer 1T-VX₂. Thus, we use only one intralayer parameter J'_0 in our effective Heisenberg model.

We proceed to employ this minimal effective Heisenberg model to understand the underlying physics of the phase transitions in twisted bilayer 1T-VX₂. Since we study 20 magnetic configurations whose energy differences are provided in the Supplemental Material (see Fig.S5)³⁸, but the effective Heisenberg model has only 7 coupling parameters, we utilized a weighted least squares method, which has also been used to determine the

Heisenberg model in iron-based superconductors⁴⁷, to determine these parameters, where the rules for the weights are as follows: (1) Since the magnetic ground states exhibit interlayer symmetry, the weight of the magnetic configurations with interlayer symmetry should be greater than that of the magnetic configurations without interlayer symmetry. (2) For magnetic configurations with interlayer symmetry, the weight of a configuration with lower energy should be greater than that of a configuration with higher energy, and similarly for those without interlayer symmetry. The specific formulas satisfying above rules for the weights are given in the Supplemental Material [Eq.(4) and Eq.(5)]³⁸. These weights ensure the error between the lowest total energies obtained from DFT calculations and predicted from above Heisenberg model less than 0.1 meV/atom. Then, the 7 couplings can be readily derived.

Figure 4(d) presents the 7 couplings of the aforementioned minimal effective Heisenberg model for twisted bilayer 1T-VSe₂ as functions of interlayer distance. As can be seen, at large interlayer distances, intralayer coupling J'_0 maintains ferromagnetic, meanwhile, all of the interlayer couplings except for J_\perp exhibit antiferromagnetic behavior (J_{OO} is negligibly small). Consequently, the system favors an intralayer ferromagnetic and interlayer antiferromagnetic ground state, namely, LAFM. In contrast, at intermediate interlayer distances, the vertically interlayer couplings, including J_\perp , J_{11} , and J_{22} , exhibit ferromagnetic characteristics, which will favor an interlayer ferromagnetic order. Meanwhile, the diagonal interlayer couplings, including J_{AO1} and J_{AO2} , maintain antiferromagnetic properties (J_{OO} is negligibly small), which suggest an interlayer antiferromagnetic order between A and other sublattices, corresponding to AFM1. At small interlayer distances, due to J_{11} and J_{22} maintaining interlayer ferromagnetism, and J'_0 being intralayer antiferromagnetic, the magnetic orders on the O1 and O2 sublattices are interlayer ferromagnetic and intralayer antiferromagnetic. Simultaneously, the strong ferromagnetic J_\perp and strong antiferromagnetic J_{AO2} result in an interlayer ferromagnetic order between overlapping V atoms (A sublattices) with an intralayer antiferromagnetic order between A and O2, namely, AFM2.

Although, twisted bilayer 1T-VS₂ has the same magnetic ground states as twisted bilayer 1T-VSe₂ at large and small interlayer distances, the ground state at intermediate distances is different. To understand this discrepancy, the couplings of the twisted bilayer 1T-VS₂ and 1T-VSe₂ at interlayer distance of 2.32Å and 2.62Å, respectively, is presented in Fig. 4(e). Obviously, the ferromagnetic intralayer coupling of J'_0 still plays a dominant role, which is different from the case of twisted bilayer 1T-VSe₂, resulting in intralayer ferromagnetism. Meanwhile, both J_\perp and J_{22} exhibit strong ferromagnetic couplings, leading to interlayer ferromagnetism. Therefore, FM is the ground state at intermediate distances for the twisted bilayer 1T-VS₂.

IV. DISCUSSION

Here, by systematically investigating the tunability of the magnetic properties in untwisted and twisted bilayer 1T-VX₂ (X = S, Se), we find that, the twisted system is easier to access richer phase transitions than untwisted one, indicating that the combination of twist and pressure provides an efficient way to tune the magnetism of layered materials. Although some studies have reported the presence of charge density wave in layered 1T-VSe₂^{45,48,49} and 1T-VS₂^{50,51}, it does not undermine the reliability of the magnetic phase transitions in twisted bilayer 1T-VX₂ (X = S, Se) demonstrated in this paper because twist can narrow the bandwidth of twisted layered materials, thereby facilitating the emergence of magnetism. For example, while bilayer graphene itself lacks of magnetism, ferromagnetism emerges in the twisted bilayer graphene^{52,53}.

We noticed that, while the detected magnetic phase transition in untwisted bilayer 1T-VX₂ was attributed to the competition between interlayer Pauli and Coulomb repulsions, which favor interlayer antiferromagnetism with short interlayer distance, and the kinetic energy, which supports interlayer ferromagnetism with large interlayer distance²¹, the magnetic phase transitions in twisted bilayer 1T-VX₂ seem to challenge this theoretical framework. We have shown that an interlayer ferromagnetic state occurs at small interlayer distances which is corresponding to strong interlayer Pauli repulsion, while an interlayer antiferromagnetic state emerges at large interlayer distances which refers to weak interlayer Pauli repulsion.

In the untwisted bilayer 1T-VX₂, the intralayer nearest-neighbor coupling J_0 remains nearly constant as the interlayer distance decreases, and the magnetic phase transition of the system arises from the competition between interlayer nearest-neighbor and next-nearest-neighbor couplings. However, in the case of twisted bilayer 1T-VX₂, the intralayer nearest-neighbor coupling J'_0 gradually changes from ferromagnetic to antiferromagnetic, playing a significant role in the magnetic phase transitions. The different behavior in intralayer nearest-neighbor hopping between untwisted and twisted cases is due to the presence of directly overlapping X atoms (from the top view) between the two X sublayers that are located within the two V sublayers after twist, resulting in the enhancement of the interactions between these overlapping X atoms, which can ultimately affects the superexchange process between intralayer V atoms. Noticeably, there are infinite numbers of twisted angles that can result in commensurate structures with presences of directly overlapping X atoms between the two X sublayers that are located within the two V sublayers after twist. The twisted angle and corresponding number of atoms in the commensurate supercell are shown in Fig.S 6 of the Supplemental Material³⁸. We argue that the twisted bilayer 1T-VX₂ which exhibits fruitful magnetic phases may be common in nature.

The twist angle plays a crucial role in tuning the properties of materials. For instance, while untwisted bilayer CrI_3 exhibits an interlayer antiferromagnetic ground state, interlayer ferromagnetic and antiferromagnetic states coexist in twisted bilayer CrI_3 with twisted angle of $\theta \leq 3^\circ$ ³⁶. At last, left-twisted ($\theta = 32.2^\circ$) and right-twisted ($\theta = 27.8^\circ$) bilayer 2H-VSe_2 show distinct responses to an electric field⁵⁴.

Since the structure of twisted bilayer 1T-VX_2 holds C_3 symmetry, our focus here is primarily on magnetic ordered configurations consistent with C_3 symmetry. Please note, we can not rule out possibility of existence of other magnetic ground states without restriction of symmetry, since one can not exhaust all antiferromagnetic configurations in the thermodynamic limit. However, even if it might happen, our conclusion, i.e. twist and pressure able to induce rich magnetic phase transitions, remains unchanged.

V. CONCLUSION

In conclusion, we systematically investigate the magnetic phase transitions of untwisted and twisted bilayer 1T-VX_2 and reveal the underlying physics based on corresponding Heisenberg model. For untwisted bilayer 1T-VX_2 , a phase transition from FM to LAFM is

found as interlayer distance decreases, which is attributed to competition between the nearest- and next-nearest-neighbor interlayer couplings. In contrast, richer magnetic phase transitions are found under pressure and the critical pressures for the phase transition are greatly reduced in twisted bilayer 1T-VX_2 compared with the untwisted case, where twisted bilayer 1T-VSe_2 undergoes phase transitions of LAFM-AFM1-AFM2 while twisted bilayer 1T-VS_2 experiences phase transitions of LAFM-FM-AFM2. It is necessary to mention that a phase transition from FM to LAFM occurs in bilayer 1T-VX_2 under twist solely. By employing an effective Heisenberg model, we find that the competition and cooperation between intralayer and interlayer couplings are responsible for the rich magnetic phase transitions in twisted bilayer 1T-VX_2 . Our results provide guidances in exploring magnetic properties of twisted layered materials.

VI. ACKNOWLEDGEMENT

This work is supported by National Natural Science Foundation of China (NOs.12004283, 12274324) and Shanghai Science and technology program(No.21JC405700). We gratefully acknowledge HZWTech for providing computation facilities.

* These authors contribute equally to the paper.

† Corresponding author. Email: yzzhang@tongji.edu.cn

¹ Cheng Gong, Lin Li, Zhenglu Li, Huiwen Ji, Alex Stern, Yang Xia, Ting Cao, Wei Bao, Chenzhe Wang, Yuan Wang, *et al.*, “Discovery of intrinsic ferromagnetism in two-dimensional van der Waals crystals,” *Nature* **546**, 265–269 (2017).

² Bevin Huang, Genevieve Clark, Efrén Navarro-Moratalla, Dahlia R Klein, Ran Cheng, Kyle L Seyler, Ding Zhong, Emma Schmidgall, Michael A McGuire, David H Cobden, *et al.*, “Layer-dependent ferromagnetism in a van der Waals crystal down to the monolayer limit,” *Nature* **546**, 270–273 (2017).

³ Yujun Deng, Yijun Yu, Yichen Song, Jingzhao Zhang, Nai Zhou Wang, Zeyuan Sun, Yangfan Yi, Yi Zheng Wu, Shiwei Wu, Junyi Zhu, *et al.*, “Gate-tunable room-temperature ferromagnetism in two-dimensional Fe_3GeTe_2 ,” *Nature* **563**, 94–99 (2018).

⁴ Xingzhi Wang, Kezhao Du, Yu Yang Fredrik Liu, Peng Hu, Jun Zhang, Qing Zhang, Man Hon Samuel Owen, Xin Lu, Chee Kwan Gan, Pinaki Sengupta, *et al.*, “Raman spectroscopy of atomically thin two-dimensional magnetic iron phosphorus trisulfide (FePS_3) crystals,” *2D Materials* **3**, 031009 (2016).

⁵ Manuel Bonilla, Sadhu Kolekar, Yujing Ma, Horacio Coy Diaz, Vijaysankar Kalappattil, Raja Das, Tatiana Eggers, Humberto R Gutierrez, Manh-Huong Phan, and Matthias Batzill, “Strong room-temperature ferromagnetism in VSe_2 monolayers on van der Waals substrates,” *Nature nanotechnology* **13**, 289–293 (2018).

⁶ Yuqiao Guo, Haitao Deng, Xu Sun, Xiuling Li, Jiyin Zhao, Junchi Wu, Wangsheng Chu, Sijia Zhang, Haibin Pan, Xusheng Zheng, *et al.*, “Modulation of metal and insulator states in 2D ferromagnetic VS_2 by van der Waals interaction engineering,” *Advanced Materials* **29**, 1700715 (2017).

⁷ Sharidya Rahman, Juan F Torres, Ahmed Raza Khan, and Yuerui Lu, “Recent developments in van der Waals antiferromagnetic 2D materials: Synthesis, characterization, and device implementation,” *ACS nano* **15**, 17175–17213 (2021).

⁸ Mongur Hossain, Biao Qin, Bo Li, and Xidong Duan, “Synthesis, characterization, properties and applications of two-dimensional magnetic materials,” *Nano Today* **42**, 101338 (2022).

⁹ Dong Chen, Wei Sun, Wenxuan Wang, Xiaoning Li, Hang Li, and Zhenxiang Cheng, “Twist-stacked 2D bilayer Fe_3GeTe_2 with tunable magnetism,” *Journal of Materials Chemistry C* **10**, 12741–12750 (2022).

¹⁰ Tingxin Li, Shengwei Jiang, Nikhil Sivadas, Zefang Wang, Yang Xu, Daniel Weber, Joshua E Goldberger, Kenji Watanabe, Takashi Taniguchi, Craig J Fennie, *et al.*, “Pressure-controlled interlayer magnetism in atomically thin CrI_3 ,” *Nature materials* **18**, 1303–1308 (2019).

¹¹ Yandong Ma, Ying Dai, Meng Guo, Chengwang Niu, Yingtao Zhu, and Baibiao Huang, “Evidence of the existence of magnetism in pristine VX_2 monolayers ($\text{X} = \text{S}, \text{Se}$) and their strain-induced tunable magnetic properties,” *ACS nano* **6**, 1695–1701 (2012).

- ¹² Jicheol Son, Brahim Marfoua, and Jisang Hong, "Strain dependent magnetic properties of 1T-VSe₂ monolayer," *Journal of the Korean Physical Society* **81**, 133–138 (2022).
- ¹³ Nathan P Wilson, Kihong Lee, John Cenker, Kaichen Xie, Avalon H Dismukes, Evan J Telford, Jordan Fonseca, Shivesh Sivakumar, Cory Dean, Ting Cao, *et al.*, "Interlayer electronic coupling on demand in a 2D magnetic semiconductor," *Nature Materials* **20**, 1657–1662 (2021).
- ¹⁴ Pingfan Gu, Yujia Sun, Cong Wang, Yuxuan Peng, Yaozheng Zhu, Xing Cheng, Kai Yuan, Chao Lyu, Xuelu Liu, Qinghai Tan, *et al.*, "Magnetic phase transitions and magnetoelastic coupling in a two-dimensional stripy antiferromagnet," *Nano Letters* **22**, 1233–1241 (2022).
- ¹⁵ Bevin Huang, Genevieve Clark, Dahlia R Klein, David MacNeill, Efrén Navarro-Moratalla, Kyle L Seyler, Nathan Wilson, Michael A McGuire, David H Cobden, Di Xiao, *et al.*, "Electrical control of 2D magnetism in bilayer CrI₃," *Nature nanotechnology* **13**, 544–548 (2018).
- ¹⁶ Bo Li, Tao Xing, Mianzeng Zhong, Le Huang, Na Lei, Jun Zhang, Jingbo Li, and Zhongming Wei, "A two-dimensional Fe-doped SnS₂ magnetic semiconductor," *Nature communications* **8**, 1958 (2017).
- ¹⁷ Wenxuan Zhu, Cheng Song, Yongjian Zhou, Qian Wang, Hua Bai, and Feng Pan, "Insight into interlayer magnetic coupling in 1T-type transition metal dichalcogenides based on the stacking of nonmagnetic atoms," *Physical Review B* **103**, 224404 (2021).
- ¹⁸ Yinghe Zhao, Lingfang Lin, Qionghua Zhou, Yunhai Li, Shijun Yuan, Qian Chen, Shuai Dong, and Jinlan Wang, "Surface vacancy-induced switchable electric polarization and enhanced ferromagnetism in monolayer metal trihalides," *Nano Letters* **18**, 2943–2949 (2018).
- ¹⁹ Rebekah Chua, Jing Yang, Xiaoyue He, Xiaojiang Yu, Wei Yu, Fabio Bussolotti, Ping Kwan Johnny Wong, Kian Ping Loh, Mark BH Breese, Kuan Eng Johnson Goh, *et al.*, "Can reconstructed se-deficient line defects in monolayer VSe₂ induce magnetism?" *Advanced Materials* **32**, 2000693 (2020).
- ²⁰ Hui Zhang, Li-Min Liu, and Woon-Ming Lau, "Dimension-dependent phase transition and magnetic properties of VS₂," *Journal of Materials Chemistry A* **1**, 10821–10828 (2013).
- ²¹ Cong Wang, Xieyu Zhou, Linwei Zhou, Yuhao Pan, Zhong-Yi Lu, Xiangang Wan, Xiaoqun Wang, and Wei Ji, "Bethe-Slater-curve-like behavior and interlayer spin-exchange coupling mechanisms in two-dimensional magnetic bilayers," *Physical Review B* **102**, 020402 (2020).
- ²² Aolin Li, Wenzhe Zhou, Jiangling Pan, Qinglin Xia, Mengqiu Long, and Fangping Ouyang, "Coupling Stacking Orders with Interlayer Magnetism in Bilayer H-VSe₂," *Chinese Physics Letters* **37**, 107101 (2020).
- ²³ Xingen Liu, Alexander P Pyatakov, and Wei Ren, "Magnetoelectric coupling in multiferroic bilayer VS₂," *Physical Review Letters* **125**, 247601 (2020).
- ²⁴ Wei Yu, Jing Li, Tun Seng Heng, Zishen Wang, Xiaoxu Zhao, Xiao Chi, Wei Fu, Ibrahim Abdelwahab, Jun Zhou, Jiadong Dan, *et al.*, "Chemically exfoliated VSe₂ monolayers with room-temperature ferromagnetism," *Advanced Materials* **31**, 1903779 (2019).
- ²⁵ Wen Zhang, Lei Zhang, Ping Kwan Johnny Wong, Jiaren Yuan, Giovanni Vinai, Piero Torelli, Gerrit van der Laan, Yuan Ping Feng, and Andrew TS Wee, "Magnetic transition in monolayer VSe₂ via interface hybridization," *ACS nano* **13**, 8997–9004 (2019).
- ²⁶ G Vinai, C Bigi, Akhil Rajan, Matthew David Watson, T-L Lee, Federico Mazzola, S Modesti, Sourabh Barua, M Ciomaga Hatnean, Geetha Balakrishnan, *et al.*, "Proximity-induced ferromagnetism and chemical reactivity in few-layer VSe₂ heterostructures," *Physical Review B* **101**, 035404 (2020).
- ²⁷ Jiang-Bin Wu, Zhi-Xin Hu, Xin Zhang, Wen-Peng Han, Yan Lu, Wei Shi, Xiao-Fen Qiao, Mari Ijiäs, Silvia Milana, Wei Ji, *et al.*, "Interface coupling in twisted multilayer graphene by resonant Raman spectroscopy of layer breathing modes," *ACS nano* **9**, 7440–7449 (2015).
- ²⁸ Kaihui Liu, Liming Zhang, Ting Cao, Chenhao Jin, Diana Qiu, Qin Zhou, Alex Zettl, Peidong Yang, Steve G Louie, and Feng Wang, "Evolution of interlayer coupling in twisted molybdenum disulfide bilayers," *Nature communications* **5**, 4966 (2014).
- ²⁹ Stephen Carr, Shiang Fang, Pablo Jarillo-Herrero, and Efthimios Kaxiras, "Pressure dependence of the magic twist angle in graphene superlattices," *Physical Review B* **98**, 085144 (2018).
- ³⁰ Felix Yndurain, "Pressure-induced magnetism in rotated graphene bilayers," *Physical Review B* **99**, 045423 (2019).
- ³¹ Xiu-Cai Jiang, Yi-Yuan Zhao, and Yu-Zhong Zhang, "Tunable band gap in twisted bilayer graphene," *Physical Review B* **105**, 115106 (2022).
- ³² Yang Gao, Xianqing Lin, Thomas Smart, Penghong Ci, Kenji Watanabe, Takashi Taniguchi, Raymond Jeanloz, Jun Ni, and Junqiao Wu, "Band Engineering of Large-Twist-Angle Graphene/h- BN Moiré Superlattices with Pressure," *Physical review letters* **125**, 226403 (2020).
- ³³ Rafi Bistritzer and Allan H MacDonald, "Moiré bands in twisted double-layer graphene," *Proceedings of the National Academy of Sciences* **108**, 12233–12237 (2011).
- ³⁴ G Trambly de Laissardiére, Didier Mayou, and Laurence Magaud, "Localization of Dirac electrons in rotated graphene bilayers," *Nano letters* **10**, 804–808 (2010).
- ³⁵ Xiu-Cai Jiang, Ze Ruan, and Yu-Zhong Zhang, "Site-selective insulating phase in a twisted bilayer hubbard model," *Physical Review B* **109**, 085104 (2024).
- ³⁶ Yang Xu, Ariana Ray, Yu-Tsun Shao, Shengwei Jiang, Kihong Lee, Daniel Weber, Joshua E Goldberger, Kenji Watanabe, Takashi Taniguchi, David A Muller, *et al.*, "Co-existing ferromagnetic–antiferromagnetic state in twisted bilayer CrI₃," *Nature Nanotechnology* **17**, 143–147 (2022).
- ³⁷ D Sahoo, S Senapati, and R Naik, "Progress and prospects of 2D VS₂ transition metal dichalcogenides," *FlatChem* , 100455 (2022).
- ³⁸ See Supplemental Material at [URL] for the structure and magnetic orders of untwisted and twisted bilayer 1T-VX₂; the Heisenberg model of the untwisted and twisted bilayer 1T-VX₂; the energy differences of different magnetic configurations for untwisted and twisted bilayer 1T-VX₂; the relationship between the total number of atoms in the commensurate supercell structure and the corresponding twist angles ($0^\circ < \theta < 60^\circ$); the twisted angles, lattice constants, number of atoms for various relatively small commensurate structures.
- ³⁹ Peter E Blöchl, "Projector augmented-wave method," *Physical review B* **50**, 17953 (1994).
- ⁴⁰ Georg Kresse and Jürgen Hafner, "Ab initio molecular-dynamics simulation of the liquid-metal–amorphous-semiconductor transition in germanium," *Physical Review B* **49**, 14251 (1994).

- ⁴¹ Georg Kresse and Jürgen Furthmüller, “Efficiency of ab-initio total energy calculations for metals and semiconductors using a plane-wave basis set,” *Computational materials science* **6**, 15–50 (1996).
- ⁴² John P Perdew, Kieron Burke, and Matthias Ernzerhof, “Generalized gradient approximation made simple,” *Physical review letters* **77**, 3865 (1996).
- ⁴³ Stefan Grimme, “Semiempirical GGA-type density functional constructed with a long-range dispersion correction,” *Journal of computational chemistry* **27**, 1787–1799 (2006).
- ⁴⁴ Sergei L Dudarev, Gianluigi A Botton, Sergey Y Savrasov, CJ Humphreys, and Adrian P Sutton, “Electron-energy-loss spectra and the structural stability of nickel oxide: An LSDA+ U study,” *Physical Review B* **57**, 1505 (1998).
- ⁴⁵ Jiagui Feng, Deepnarayan Biswas, Akhil Rajan, Matthew D Watson, Federico Mazzola, Oliver J Clark, Kaycee Underwood, Igor Markovic, Martin McLaren, Andrew Hunter, *et al.*, “Electronic structure and enhanced charge-density wave order of monolayer VSe₂,” *Nano letters* **18**, 4493–4499 (2018).
- ⁴⁶ Qingqing Ji, Cong Li, Jingli Wang, Jingjing Niu, Yue Gong, Zhepeng Zhang, Qiyi Fang, Yu Zhang, Jianping Shi, Lei Liao, *et al.*, “Metallic vanadium disulfide nanosheets as a platform material for multifunctional electrode applications,” *Nano letters* **17**, 4908–4916 (2017).
- ⁴⁷ JK Glasbrenner, II Mazin, Harald O Jeschke, PJ Hirschfeld, RM Fernandes, and Roser Valentí, “Effect of magnetic frustration on nematicity and superconductivity in iron chalcogenides,” *Nature Physics* **11**, 953–958 (2015).
- ⁴⁸ Adolfo O Fumega, Marco Gobbi, Paul Dreher, Wen Wan, Carmen González-Orellana, Marina Peña-Díaz, Celia Rogero, J Herrero-Martín, Pierluigi Gargiani, Max Ilyn, *et al.*, “Absence of ferromagnetism in VSe₂ caused by its charge density wave phase,” *The Journal of Physical Chemistry C* **123**, 27802–27810 (2019).
- ⁴⁹ Paula Mariel Coelho, Kien Nguyen Cong, Manuel Bonilla, Sadhu Kolekar, Manh-Huong Phan, José Avila, Maria C Asensio, Ivan I Oleynik, and Matthias Batzill, “Charge density wave state suppresses ferromagnetic ordering in VSe₂ monolayers,” *The Journal of Physical Chemistry C* **123**, 14089–14096 (2019).
- ⁵⁰ Hyuk Jin Kim, Byoung Ki Choi, In Hak Lee, Min Jay Kim, Seung-Hyun Chun, Chris Jozwiak, Aaron Bostwick, Eli Rotenberg, and Young Jun Chang, “Electronic structure and charge-density wave transition in monolayer VS₂,” *Current Applied Physics* **30**, 8–13 (2021).
- ⁵¹ Camiel Van Efferen, Jan Berges, Joshua Hall, Erik Van Loon, Stefan Kraus, Arne Schobert, Tobias Wekking, Felix Huttmann, Eline Plaar, Nico Rothenbach, *et al.*, “A full gap above the Fermi level: the charge density wave of monolayer VS₂,” *Nature Communications* **12**, 6837 (2021).
- ⁵² Aaron L Sharpe, Eli J Fox, Arthur W Barnard, Joe Finney, Kenji Watanabe, Takashi Taniguchi, MA Kastner, and David Goldhaber-Gordon, “Emergent ferromagnetism near three-quarters filling in twisted bilayer graphene,” *Science* **365**, 605–608 (2019).
- ⁵³ Guorui Chen, Aaron L Sharpe, Eli J Fox, Ya-Hui Zhang, Shaoxin Wang, Lili Jiang, Bosai Lyu, Hongyuan Li, Kenji Watanabe, Takashi Taniguchi, *et al.*, “Tunable correlated Chern insulator and ferromagnetism in a moiré superlattice,” *Nature* **579**, 56–61 (2020).
- ⁵⁴ Yu-Hao Shen, Wen-Yi Tong, He Hu, Jun-Ding Zheng, and Chun-Gang Duan, “Exotic dielectric behaviors induced by pseudo-spin texture in magnetic twisted bilayer,” *Chinese Physics Letters* **38**, 037501 (2021).